applied sciences

MDPI

Article

Quaternion Signal Analysis for Detection of Broken Rotor Fault Degrees in Induction Motors

Jose Luis Contreras-Hernandez *, Dora Luz Almanza-Ojeda, Rogelio Castro-Sanchez and Mario Alberto Ibarra-Manzano

Telematics and Digital Signal Processing Research Groups (CAs), Electronics Engineering Department, DICIS, University of Guanajuato, Salamanca 36885, Mexico; dora.almanza@ugto.mx (D.L.A.-O.); castro@ugto.mx (R.C.-S.); ibarram@ugto.mx (M.A.I.-M.)

* Correspondence: jose.contreras@ugto.mx; Tel.: +52-464-647-9940

Abstract: Fault detection in induction motors is essential for maintaining the reliability of industrial operations. In practical applications, induction motors experience gradual wear on critical components, such as rotor bars, affecting their performance. This paper introduces a new methodology for modeling predictive wear functions related to rotor faults in induction motors, providing accurate forecasts and optimal performance through Quaternion Signal Analysis in the time domain. Our approach accurately detects wear in broken rotor bars and anticipates their degradation over time. The methodology involves coupling four vibration signals from the motor, representing them as quaternion coefficients, and calculating their rotational attributes to derive a statistical mean. We employ polynomial and Fourier regression techniques to construct a predictive wear function. We assess its accuracy through root mean square error (RMSE) analysis, which improves with increased sample size and regression complexity. Our findings indicate that polynomial regression, particularly at the second degree, achieves superior RMSE results compared to Fourier regression, even within limited sample windows. This approach offers a robust framework for early fault detection and wear prediction in induction motors, supporting enhanced maintenance strategies.

Keywords: bar quantification; induction motor fault; QSA; quaternions; regression

check for updates

Academic Editors: Jose M. Guerrero, Araitz Iturregi, Sergio Toscani and Gerard Ghibaudo

Received: 2 December 2024
Revised: 18 January 2025
Accepted: 7 February 2025
Published: 10 February 2025

Citation: Contreras-Hernandez, J.L.; Almanza-Ojeda, D.L.; Castro-Sanchez, R.; Ibarra-Manzano, M.A. Quaternion Signal Analysis for Detection of Broken Rotor Fault Degrees in Induction Motors. *Appl. Sci.* **2025**, *15*, 1787. https://doi.org/10.3390/app15041787

Copyright: © 2025 by the authors. Licensee MDPI, Basel, Switzerland. This article is an open access article distributed under the terms and conditions of the Creative Commons Attribution (CC BY) license (https://creativecommons.org/licenses/by/4.0/).

1. Introduction

Induction motors are important electric machines in industry processes and must be kept in optimal operation. Signal analysis techniques are essential for early fault detection in rotating machinery, helping to prevent unexpected downtime, economic losses, and potential major failures [1,2]. Common faults in induction motors include bearing defects [3], stator winding failures, air-gap eccentricity, unbalanced bars, and broken rotor bar (BRB) faults [4]. BRB faults are particularly significant in the literature due to their high risk of causing additional damage [5]. Numerous methodologies have been developed to detect or characterize BRB faults, focusing on spectral analysis, machine learning, and statistical approaches [6].

Spectral analysis methods involve extensive data processing and are primarily oriented toward fault detection and classification. Fourier and wavelet transforms are methodologies in spectral analysis valued for their ability to associate specific signal frequencies with BRB faults. In addition, studies in the literature often integrate statistical analysis into spectral techniques to enhance fault detection accuracy, as in [7], where a methodology combining the digital Taylor–Fourier transform (DTFT) with variance analysis effectively identified

rotor bar wear across states ranging from healthy to BRB. In wavelet algorithms, the authors of [8] successfully classified multiple BRB faults by extracting statistical features directly from raw signals using advanced techniques such as Matching Pursuit (MP) and Discrete Wavelet Transform (DWT). Moreover, several studies leverage machine learning methods like k-Nearest Neighbor (KNN) and support vector machines (SVMs) for BRB classification. For instance, the approach in [9] integrates Discrete Wavelet Transform (DWT) with these machine learning algorithms to achieve robust multi-class BRB classifications.

Recently, there has been a surge of interest in utilizing machine learning and deep learning techniques for fault detection in induction motors. This trend reflects these approaches' proven accuracy and efficiency in identifying and diagnosing faults, marking significant progress in predictive maintenance [6]. Specifically, for BRB fault detection using time-domain signals, studies such as [10] have explored various machine learning algorithms—including fuzzy ARTMAP networks, SVM, KNN, and Multilayer Perceptron (MLP) networks—without requiring prior domain knowledge. This adaptability underscores the capability of machine learning methods to capture complex patterns related to BRB faults. Additionally, ref. [11] presents an innovative algorithm that classifies BRB conditions by applying statistical metrics derived from motor vibration signals, such as kurtosis, skewness, and variance. These metrics are then processed through classifiers like Naive Bayes, MLP, SVM, and Optimum-Path Forest, further demonstrating the efficacy of machine learning in accurate BRB fault classification. In [12], homogeneity and kurtosis metrics were employed to classify motor conditions, from healthy states to the presence of two BRBs, using a backpropagation artificial neural network. This approach demonstrates the power of neural networks in identifying complex data patterns and accurately diagnosing motor faults. Similarly, ref. [13] leveraged stator current signals to obtain comprehensive two-dimensional insights into BRB severity across time and frequency domains, calculating entropy at various load levels to assess fault impact. Conversely, in [14], the authors proposed a degradation model for BRB faults by applying principal component analysis (PCA). Using raw torque, stator current, and speed signals, they estimated the remaining useful life of the BRBs, highlighting PCA's utility in modeling the degradation process.

The works presented above classify BRB using methods that involve a certain level of complexity and require significant computational resources. Utilizing quaternions could simplify this process, as they provide a unique mathematical framework because they are an extension of complex numbers, consisting of a real part and a three-dimensional vector of imaginary components [15]. This distinctive configuration has spurred interest across various fields, revealing quaternions' versatility and potential in advanced applications. For example, in image processing, quaternions have been shown to facilitate image enhancement and manipulation in ways that surpass conventional methods [16], offering new data representation and transformation possibilities. In robotic motion tracking, as detailed in [17], quaternions provide a sophisticated framework for accurately monitoring and controlling robot movement, delivering the precision essential for executing complex tasks. In control systems, quaternions are equally valuable, enabling the design of robust control mechanisms with high accuracy and reliability [18]. The versatility of quaternions in various domains highlights their impact on advancing technological innovation. In spectral analysis, quaternions have been effectively combined with the Fourier Transform, as demonstrated in [19], to perform comprehensive spectral analysis of three-phase currents in induction motors, achieving a bearing fault classification accuracy of approximately 94.2%. Likewise, in [20], researchers developed the Quaternion Empirical Wavelet Transform (QEWT) based on the Quaternion Fourier Transform to diagnose outer ring, inner ring, and rolling bearing faults, illustrating quaternions' capability in high-precision fault detection.

We have demonstrated the versatility of quaternions in previous works as [21,22], where we employed Quaternion Signal Analysis (QSA) to detect multiple faults and their combinations in induction motors. This methodology involves rotating quaternion signals and performing statistical analyses, calculating mean, variance, kurtosis, skewness, standard deviation, root mean square, and shape factor. Subsequently, machine learning techniques are applied to classify various fault conditions and combinations. This approach highlights the effectiveness of QSA in capturing and classifying complex fault patterns. Similarly, the QSA was used in [23] to diagnose short-circuit damage in transformer windings demonstrating that this method is not exclusive to classifying faults in induction motors. QSA has shown high accuracy in fault classification through simple mathematical operations in the time domain, even using four statistical values from three-phase currents as in [24], where four levels of inter-turn short circuit faults per phase and healthy states were classified.

On the other hand, regression methods utilize statistical processes to model relationships between variables, providing simplicity and low computational costs, especially with polynomial regressions. Furthermore, techniques like Fourier regressions can improve the effectiveness of stepped models. Studies have introduced methodologies for modeling predictive wear functions capable of quantifying BRB faults providing accurate forecasts and optimal performance as in [25]. In this, the authors present regression-based methods to evaluate BRB degradation using curve-fitting techniques such as linear, polynomial, and least squares regression with a power law. The method utilizes fault sideband parameters from the current spectrum, machine rating, and load torques of 50%, 75%, and 100% to gauge BRB severity levels from one to six, providing a structured model for fault severity assessment.

As BRB faults in induction motors develop gradually, establishing an effective model to predict future behavior with straightforward calculations becomes crucial. This approach not only helps prevent severe damage but also ensures timely maintenance, safeguarding your equipment and investment. Our method combines QSA with statistical feature analysis and polynomial and Fourier regressions to deliver reliable, practical predictive wear functions for motor maintenance. The proposed method utilizes four vibration signals with 29,999 samples measured from an induction motor operating at steady state and full load (100%): tangential mechanical vibration speed in the housing (V_h), axial mechanical vibration speed on the driven side (V_a), radial mechanical vibration speed on the non-driven side (V_s), and radial mechanical vibration speed on the driven side (V_d). The use of four signals to adapt them to the quaternions allows us to analyze different elements of the motor in various axes. This approach allows us to cover more variables, which may reflect the characteristics of the analyzed failures. However, a disadvantage of using quaternions is that they require four signals, which means that it is necessary to use at least two or more sensors. Not all databases have access to this number of sensors, which can limit the analysis. The method is evaluated across motor conditions ranging from healthy states to one, two, and three BRB faults, demonstrating its effectiveness in fault quantification and progression tracking.

This paper is structured into four sections: Section 1 introduces BRB fault detection. Section 2 describes the background of QSA and statistical methodology. Section 3 presents and discusses the results, comparing the results of polynomial and Fourier regressions. Finally, Section 4 presents conclusions and future work.

2. Methodology

As BRB faults in induction motors develop gradually, establishing an effective model to predict future behavior with straightforward calculations becomes crucial. This approach

not only helps prevent severe damage but also ensures timely maintenance, safeguarding your equipment and investment. By modeling quaternion-based statistical features, the proposed method characterizes BRB through predictive wear functions from a healthy motor state to three BRBs. Unlike traditional approaches that provide only discrete fault levels, this model enables a continuous fault severity assessment. The algorithm comprises two main stages: (1) the Quaternion Signal Analysis (QSA) method and (2) the fitting and evaluation procedures. Figure 1 illustrates the method's flowchart for detecting BRB severity, utilizing four vibration signals as input. Each stage of the method, as shown in Figure 1, is detailed in the following subsections.

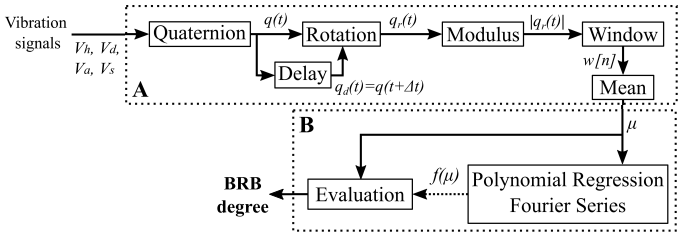


Figure 1. Proposed workflow diagram. (**A**) QSA method. (**B**) Fitting and evaluation procedures.

2.1. QSA Method

Quaternions model the three-dimensional movements of a point in space. In a complementary way, the QSA method allows modeling the signals that generate the movements, facilitating a multidimensional analysis adapted to spatial and temporal problems. This approach detects spatial signatures using quaternion arithmetic and temporal signatures by estimating statistical displacement models. Combining both elements enables the method to achieve greater precision and robustness in fault detection than the classic techniques.

This section outlines the methodology for defining quaternion signals and calculating their rotations. Subsequently, our approach computes modulus and statistical measures based on these rotations. The quaternion q is constructed as shown in (1), using the coefficients q_0, q_1, q_2, and q_3 [26].

$$q = q_0 + q_1 i + q_2 j + q_3 k \tag{1}$$

The quaternion signal $q(t)$ shown in section A of Figure 1 is constructed from the vibration signals $V_h(t)$, $V_d(t)$, $V_a(t)$, and $V_s(t)$, as formulated in (2). Signals $V_h(t)$, $V_d(t)$, and $V_a(t)$ were chosen to assess vibrations along the x-, y-, and z-axes of the induction motor, while $V_s(t)$ provides insight into rear motor vibrations. By selecting signals from different motor sections, our methodology enables a more comprehensive analysis, as Quaternion Signal Analysis (QSA) integrates the distinct characteristics of each signal. The vibration signals are represented discreetly with a total of 29,999 samples.

$$q(t) = V_h(t) + V_d(t)i + V_a(t)j + V_s(t)k \tag{2}$$

Then, the shifted quaternion signal $q_d(t)$ is obtained by the displacement of Δt samples in $q(t)$. Equation (3) presents the equality [22].

$$q_d(t) = q(t + \Delta t) \tag{3}$$

The coefficients V_{hd}, V_{dd}, V_{ad}, and V_{sd} form the quaternion $q_d(t)$ shown in Figure 1 with 29,998 samples, as defined in (4). These coefficients are the vibration coefficients V_h, V_d, V_a, and V_s in $t + \Delta t$.

$$q_d(t) = V_{hd}(t) + V_{dd}(t)i + V_{ad}(t)j + V_{sd}(t)k \tag{4}$$

A quaternion model can represent the transition from a current quaternion sample, q, to a delayed quaternion sample, q_d. This means that we can identify the quaternion model that enables q to achieve the values of q_d through quaternion rotation operations, as illustrated in Figure 2.

Rotation quaternions represent three-dimensional rotations and they are related to the axis and angle. Based on Euler's rotation theorem, any rotation can be defined using unit vectors $\hat{x}, \hat{y}$, and $\hat{z}$ and angle θ. The axis-angle components can be converted into components of a rotation quaternion q_r by Equations (5)–(8).

$$q_{r0} = \cos\left(\frac{\theta}{2}\right) \tag{5}$$

$$q_{r1} = \hat{x}\sin\left(\frac{\theta}{2}\right) \tag{6}$$

$$q_{r2} = \hat{y}\sin\left(\frac{\theta}{2}\right) \tag{7}$$

$$q_{r3} = \hat{z}\sin\left(\frac{\theta}{2}\right) \tag{8}$$

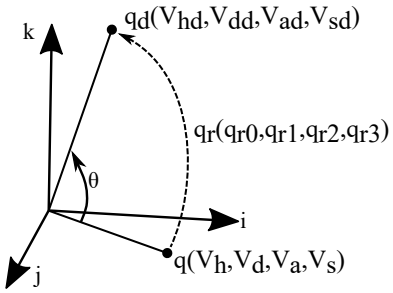


Figure 2. Rotation of $q(t)$ to obtain $q_d(t)$.

The above-mentioned process generates a rotated quaternion for each sample and its corresponding delayed value. This operation is applied to all samples of the signals to characterize the rotational behavior of the signal over time.

Taking into account the above described, q and q_d are algebraically related by (9) [21], where q_r^{-1} is the inverse of rotation quaternion.

$$q_d = q_r \otimes q \otimes q_r^{-1} \tag{9}$$

The operator $\otimes$ refers to the Hamilton product which is described as in (10).

$$\begin{aligned} q_r \otimes q = {} & (q_{r0}V_h - q_{r1}V_d - q_{r2}V_a - q_{r3}V_s) \\ & +(q_{r0}V_d + q_1V_h + q_{r2}V_s - q_{r3}V_a)i \\ & +(q_{r0}V_a - q_1V_s + q_{r2}V_h - q_{r3}V_d)j \\ & +(q_{r0}V_s + q_1V_a - q_{r2}V_d + q_{r3}V_h)k. \end{aligned} \tag{10}$$

By the properties of quaternions, the relation of q_r, q_d, and q can be written as (11) [23].

$$q_d(t) = q_r(t) \cdot q(t) \tag{11}$$

This means that if we know the values of q and q_d, we can obtain q_r through the product of general rotation matrix and q presented in (12) [21] using the coefficients values shown in (2) and (4). This value contains the two-sample quaternion model, which helps us obtain statistical values of multiple models to quantify BRBs later.

$$q_r = \begin{bmatrix} 1-2V_{ad}^2-2V_{sd}^2 & 2(V_{dd}V_{ad}+V_{hd}V_{sd}) & 2(V_{dd}V_{sd}-V_{hd}V_{ad}) \\ 2(V_{dd}V_{ad}-V_{hd}V_{sd}) & 1-2V_{dd}^2-2V_{sd}^2 & 2(V_{ad}V_{sd}+V_{hd}V_{dd}) \\ 2(V_{dd}V_{sd}+V_{hd}V_{ad}) & 2(V_{ad}V_{sd}-V_{hd}V_{dd}) & 1-2V_{dd}^2-2V_{ad}^2 \end{bmatrix} \begin{bmatrix} V_d \\ V_a \\ V_s \end{bmatrix} \quad (12)$$

Next, we compute and organize the rotational models for the signal based on the pure quaternion $q_r(t)$ as defined in (13) [23]. Here, q_{r0} is set to zero, reflecting that the rotation is confined to the three-dimensional space of the imaginary components.

$$q_r(t) = q_{r1}(t)i + q_{r2}(t)j + q_{r3}(t)k \quad (13)$$

We have vibration signals containing 29,999 samples, and the quaternion q_r is calculated for each sample with the next one, resulting in 29,998 pure quaternions. After this, we calculate the modulus of each quaternion using Equation (14), which generates a constant value for each one.

$$|q_r| = \sqrt{q_{r1}^2 + q_{r2}^2 + q_{r3}^2} \quad (14)$$

Using these values of consecutive models from $q_r(t)$, we can assemble a vector **w**[n] by selecting N samples from the signals as in (15) [15], where $t + N\Delta t$ refers to the sample of the rotation obtained.

$$\mathbf{w}[n] = [|q_r(t)|, |q_r(t+\Delta t)|, |q_r(t+2\Delta t)| \ldots |q_r(t+N\Delta t)|] \quad (15)$$

Statistical analysis of **w**[n] is essential for quantitatively characterizing the models and defining diagnostic value ranges for each BRB condition. Following the workflow in Figure 1, the mean (μ) was selected as the statistical measure with the best-fitting performance. The mean of **w**[n] reflects the evolution of signals over time and is calculated according to (16).

$$\mu = \frac{1}{N}\sum_{n=1}^{N} \mathbf{w}[n] \quad (16)$$

Each test file for each BRB condition contains 29,999 samples, providing 29,998 moduli of $q_r(t)$. The window **w**[n] utilizes N values from these 29,998 moduli to compute μ. By shifting the window **w**[n] across the test file, multiple values of μ can be calculated. This approach enables calculating and evaluating polynomial and Fourier models that describe BRB behavior, as shown in Section 2 of Figure 1.

2.2. Fitting and Evaluation

The values of μ are derived from test files corresponding to a healthy motor, one BRB, two BRBs, and three BRBs to model the function $f(\mu)$ using polynomial regression and Fourier series. This function quantitatively assesses the BRB damage level in the induction motor. Polynomial regressions and the Fourier series were calculated in the second to ninth order, which is the range supported by Matlab's function capabilities. Results from the second to sixth order are presented, as higher-order fits produce similar algebraic expressions and accuracy, making them unnecessary for further consideration.

The remaining files are evaluated in $f(\mu)$ by calculating μ to determine the extent of BRB damage. Figure 3 displays the fitted functions generated through polynomial and Fourier series methods, comparing these fitted functions with the actual data samples. The boxplot graphs present position results from one file for each fault state, analyzed using a fitted function. They distinctly showcase the minimum and maximum values, as well as the mean, providing clear insights into the data. As anticipated, the estimated

curves closely align with the observed data, achieving the accuracy required for reliable damage assessment.

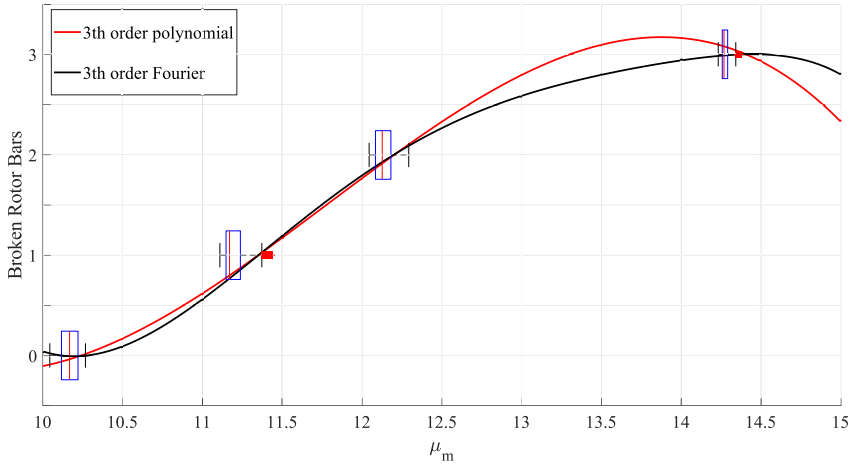


Figure 3. Polynomial and Fourier regressions.

2.3. Experimental Setup

Our work is tested with a dataset of the workbench presented in [27] to validate its effectiveness. The experimental setup, illustrated in Figure 4, includes a three-phase induction motor and a direct current machine acting as a generator to simulate load torque. They are connected by a shaft with a rotary torque wrench. Additionally, various sensors are connected at different locations within the setup.

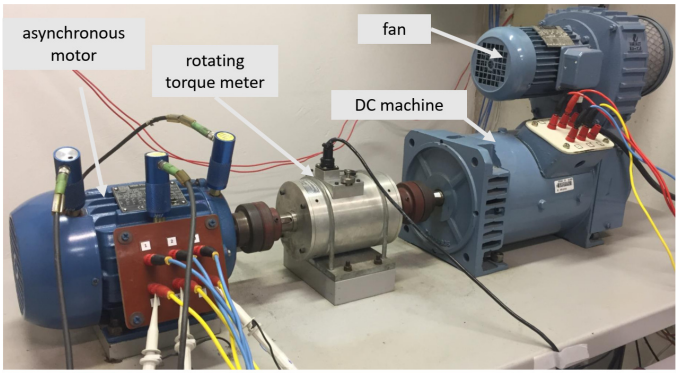


Figure 4. Experimental setup of the induction motor with one, two, and three BRBs [27].

The workbench consists of vibration, current, and voltage measurements from which we selected four vibration measurements. These are taken from various induction motor parts to analyze its mechanical behavior. This analysis enables the adaptation of four signals into a quaternion format. In past studies [22,23], a combination of current and mechanical vibration signals was utilized due to a scarcity of signals. However, this work aims to use signals of the same type for a more consistent analysis.

These four signals are acquired by four vibrocontrol uniaxial accelerometers model PU2001, located on the housing, on the driven side, and on the non-driven side to obtain tangential, radial, and axial vibration. The sensors present a sensitivity of 10 mV/mm/s, with a frequency range from 5 to 2000 Hz. The data acquisition system utilized in the experimental setup is a National Instruments (Austin, TX, USA) data acquisition card, model NI DAQmx PCIe-6259. This card features 32 analog input channels, each with a resolution of 16 bits and an acquisition rate of 1.25 MHz. Additionally, it includes four channels of 16-bit analog output, operating at a speed of 2.8 MHz, and 48 digital I/O channels capable of functioning at a clock frequency of up to 10 MHz.

The signals V_h, V_d, V_a, and V_s are acquired from a three phase induction motor of the W22 standard line from manufacturer WEG, with 1 hp, 220 V/380 V, 3.02 A/1.75 A, four poles, 34 rotor bars in the squirrel cage rotor, a rated speed of 1715 rpm, and a nominal torque of 4.1 Nm. The database includes two additional vibration signals. These signals were tested using various combinations, but the resulting statistics were insufficient for proper characterization. Therefore, the signals that yielded the best results were those recorded from the engine chassis. Different directional measurements were selected to enhance the results. The placement of the sensors and the orientation of the signals are shown in Figure 5.

The induction motor is driven by a control panel, for which the type of drive can be selected as star or triangle, and the type of supply as direct mains voltage or via a three-phase inverter. A shaft containing a rotary torque wrench Transtec model MT-103 (Arlington, VA, USA) connects the motor with a direct-current machine, simulating the load in the motor of 100% of full load in all tests.

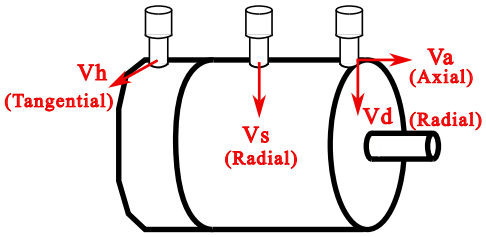


Figure 5. The position of the sensors and the orientation of the signals.

The workbench shows between one and four adjacent rotor bar failures caused by 6 mm diameter drilling in the squirrel cage rotor to ensure that the rotor bar was completely drilled alongside the healthy state by means of a bench drill mounted with the tip centered at half the longitudinal length of the rotor, as is shown in Figure 6.

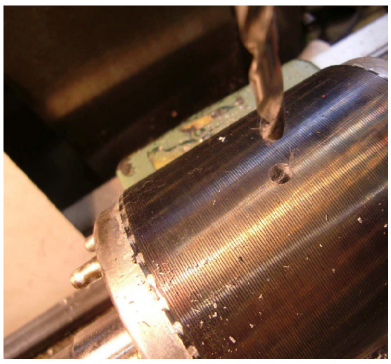


Figure 6. Provoked BRB drilling [27].

We selected the sets of healthy and from one to three BRBs because they presented a gradual increase in the results, while the four BRB states provoked regressions with instability.

The dataset presents ten repetitions of each state acquired during 18 s with a sample rate of 8.326 kHz. We selected thirty thousand samples in a steady state of the four vibration signals to test.

3. Results

In the experimental tests, a random test file from each rotor state was selected to create a sub-workbench for calculating $f(\mu_w)$. Our method then adapts one sample from each of the four vibration signals to construct the current quaternion $q(t)$ and determines the rotation $q_r(t)$ based on the previous quaternion sample $q_d(t)$, as shown in (12). By

calculating the modulus of $q_r(t)$ for each delayed quaternion sample, we obtain a total of 29,999 samples.

Multiple shifted windows $w[n]$—utilizing 4000, 6000, 8000, 10,000, 12,000, 14,000, and 20,000 samples—are employed to calculate the mean (μ) for each window, forming a function $f(\mu)$ that characterizes fault behavior. This model function is then evaluated on the remaining test files (excluding those used in model formation). The dispersion of data points around the fitted function can be measured by root mean square error (RMSE), allowing us to evaluate how closely the data are concentrated around the fitted function [28]. We consider this measurement to be a metric to record the joint accuracy of our method across different rotor states. The process is repeated forty times using the original dataset with polynomial regression and Fourier series. The mean RMSE values from these forty trials are analyzed across polynomial orders from second to sixth.

Figure 7 shows the average of the RMSE values obtained from the forty tests, with the different window samples tested along with multiple orders of the predictive wear functions. Analyzing the graph mentioned above, it is observed that as window size increases, the mean RMSE values remain relatively stable for each polynomial order, indicating that sample size has minimal impact on the efficiency of our method at a given order.

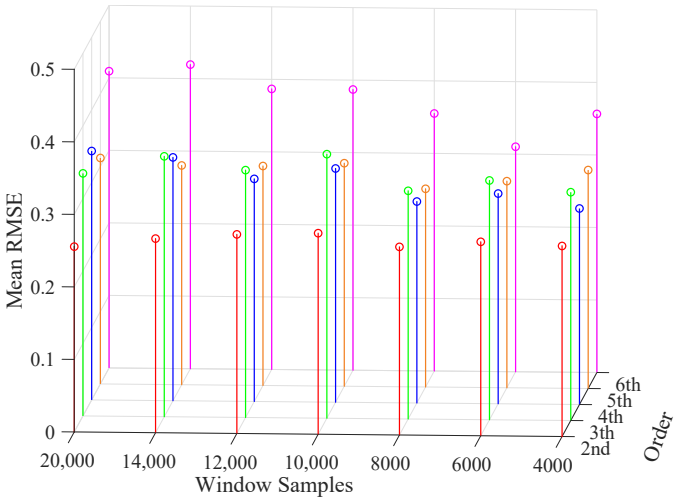


Figure 7. Mean RMSE behavior with polynomial modeling.

Table 1 presents the average of the RMSE for each window size and polynomial order, along with the minimum and maximum RMSE values across repetitions. The lowest average of the RMSE observed is 0.256, achieved with 20,000 window samples in the second order, though a comparable result is obtained with 8000 samples, yielding a mean RMSE of 0.259 in the same order. In the sixth order, mean RMSE increases in all cases due to a broader spread in minimum and maximum values. Polynomial regression demonstrates consistent behavior, largely unaffected by sample size or polynomial order.

Similarly, we calculated the mean of forty RMSE results to examine the behavior of the Fourier series as a regression method, ranging from the second to the sixth order. Figure 8 illustrates these results, showing that the method's efficiency is impacted by sample size, particularly from the fourth to the sixth order. While the Fourier series modeling displays consistent behavior at lower orders, its performance varies as the order increases.

Table 1. Mean, minimum, and maximum RMSE in each order using polynomial modeling.

Window Samples	Order 2	3	4	5	6
	Mean (min, max)	***Mean (min, max)***	***Mean (min, max)***	***Mean (min, max)***	***Mean (min, max)***
4000	0.263 (0.22, 0.39)	0.315 (0.22, 0.47)	0.270 (0.17, 0.47)	0.301 (0.20, 0.56)	0.357 (0.17, 1.29)
6000	0.267 (0.21, 0.34)	0.330 (0.21, 0.66)	0.290 (0.19, 0.56)	0.285 (0.18, 0.66)	0.310 (0.15, 0.66)
8000	0.259 (0.22, 0.32)	0.315 (0.20, 0.80)	0.278 (0.17, 0.74)	0.273 (0.17, 0.68)	0.355 (0.17, 0.88)
10,000	0.277 (0.22, 0.47)	0.364 (0.21, 0.78)	0.322 (0.18, 0.79)	0.308 (0.18, 0.65)	0.387 (0.15, 1.41)
12,000	0.274 (0.22, 0.47)	0.341 (0.21, 0.83)	0.307 (0.18, 0.85)	0.303 (0.18, 0.68)	0.387 (0.18, 1.08)
14,000	0.268 (0.21, 0.50)	0.359 (0.20, 0.71)	0.335 (0.19, 0.76)	0.302 (0.18, 0.59)	0.419 (0.14, 0.93)
20,000	0.256 (0.21, 0.43)	0.334 (0.20, 0.81)	0.343 (0.17, 0.86)	0.312 (0.18, 0.79)	0.409 (0.17, 0.96)

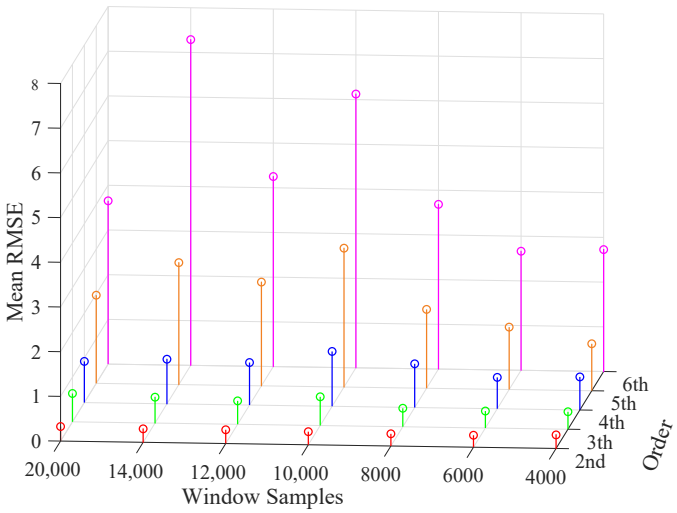


Figure 8. Mean RMSE behavior with Fourier series modeling.

Table 2 presents the mean RMSE for each window size and modeling order, along with the minimum and maximum RMSE values across forty repetitions. The lowest mean RMSE observed in the table is 0.268, achieved with 6000 window samples in the second order. It has been observed that the difference between the minimum and maximum values of orders is greater than the fourth order increases when using Fourier series modeling. Additionally, the average values of the RMSE for these orders change differently compared to those using polynomial modeling. This indicates that the functions derived from the Fourier series have less adaptation to the verification values.

Comparing the average of the RMSE values in Tables 1 and 2 reveals that increasing the number of samples minimally impacts the mean RMSE across each order. However, polynomial modeling consistently yields a lower mean RMSE, indicating that the function $f(\mu)$ achieves a closer fit to the original values and exhibits stable results as the order and window sample parameters increase. The polynomial method yields more stable values. Therefore, even when different samples are used to create the function that describes the behavior of the bars, the resulting functions adapt more effectively compared to those generated by the Fourier series. While a lower order in Fourier series with fewer samples may produce similar values in variation, the polynomial method generally demonstrates better adaptability.

Table 2. Mean, minimum, and maximum RMSE in each order from two to six using Fourier series modeling.

Window	Order				
	2	3	4	5	6
Samples	***Mean (min, max)***	***Mean (min, max)***	***Mean (min, max)***	***Mean (min, max)***	***Mean (min, max)***
4000	0.303 (0.16, 0.66)	0.391 (0.16, 1.28)	0.739 (0.18, 3.06)	1.051 (0.17, 4.48)	2.727 (0.07, 19.73)
6000	0.268 (0.19, 0.53)	0.379 (0.17, 1.34)	0.702 (0.16, 3.11)	1.396 (0.18, 6.00)	2.663 (0.12, 36.69)
8000	0.273 (0.16, 0.69)	0.414 (0.15, 2.45)	0.978 (0.23, 7.26)	1.765 (0.14, 12.63)	3.684 (0.12, 68.57)
10,000	0.293 (0.17, 0.70)	0.643 (0.16, 3.60)	1.227 (0.18, 4.69)	3.107 (0.21, 26.46)	6.125 (0.11, 81.33)
12,000	0.308 (0.18, 0.74)	0.524 (0.17, 4.67)	0.951 (0.18, 8.13)	2.321 (0.15, 26.73)	4.252 (0.10, 80.28)
14,000	0.301 (0.17, 0.64)	0.579 (0.14, 3.13)	0.998 (0.16, 4.89)	2.728 (0.17, 20.43)	7.288 (0.09, 162.18)
20,000	0.325 (0.18, 0.70)	0.634 (0.15, 3.37)	0.921 (0.15, 5.55)	1.972 (0.15, 21.71)	3.653 (0.09, 29.71)

A lower order results in fewer operations during modeling and the QSA method demonstrates that a higher order is not necessary to achieve good adaptation results with the functions. Additionally, it has been shown that, given a sampling rate of 8.326 kHz, a duration of less than one second is sufficient in a real-world scenario to obtain a diagnosis of the wear degree in rotor bars.

4. Conclusions

Few studies have developed methodologies to quantify gradual levels of faults, such as BRB faults, in induction motors. The method presented here accurately quantifies BRB failure severity using Quaternion Signal Analysis (QSA), polynomial regression, and Fourier series modeling. This approach provides incremental records of motor behavior, enabling precise estimation and timely prevention of severe faults in the time domain.

The mean RMSE results indicate consistent performance across regression orders, window sample sizes, and modeling techniques. Polynomial modeling, in particular, demonstrates that changes in function order and window size have minimal impact on method effectiveness. This robustness allows for low-order and low-sample implementations, which are computationally efficient as they rely solely on fundamental addition and multiplication operations, unlike Fourier series, which require sine and cosine harmonics.

Future work will test this methodology by expanding the number of BRB conditions to detect partial BRBs and validating it with breaks in the junction between the bar and the side rings. In addition, we are interested in applying our development to assess wear levels in various rotating machine components, such as bearings and gearboxes, to validate their performance across diverse failure sources.

The QSA method was designed to adapt to different load conditions in induction motors; however, this adaptability needs to be validated. Consequently, we will conduct an analysis to examine how the ability to detect fault signatures depends on various load levels in the induction motor.

Author Contributions: Conceptualization, J.L.C.-H. and M.A.I.-M.; methodology, J.L.C.-H. and D.L.A.-O.; software, J.L.C.-H.; validation, D.L.A.-O. and R.C.-S.; formal analysis, J.L.C.-H. and M.A.I.-M.; investigation, J.L.C.-H.; resources, M.A.I.-M.; data curation, D.L.A.-O.; writing—original draft preparation, J.L.C.-H.; writing—review and editing, D.L.A.-O. and M.A.I.-M.; visualization, J.L.C.-H. and R.C.-S.; supervision, R.C.-S.; funding acquisition, M.A.I.-M. All authors have read and agreed to the published version of the manuscript.

Funding: The APC was funded by the Electronic Engineering Department of Universidad de Guanajuato under POA 2024.

Institutional Review Board Statement: Not applicable.

Informed Consent Statement: Not applicable.

Data Availability Statement: The original contributions presented in the study are included in the article, further inquiries can be directed to the corresponding author.

Acknowledgments: The authors thank the University of Guanajuato for the facilities and support to develop this project. Special thanks to the DAIP CIIC 048/2024 project: "Implementation of an Automatic Braking System for Electric Vehicles for People with Disabilities" (valid from 1 January to 31 December 2024) for its financial and technical support.

Conflicts of Interest: The authors declare no conflicts of interest. The funders had no role in this study's design, in the collection, analyses, or interpretation of data, in the writing of the manuscript, or in the decision to publish the results.

Abbreviations

The following abbreviations are used in this manuscript:

BRB	Broken Rotor Bar
FFT	Fast Fourier Transform
MUSIC	Multiple Signal Classification
DTFT	Digital Taylor–Fourier Transform
MP	Matching Pursuit
KNN	k-Nearest Neighbor
SVM	Support Vector Machine
DWT	Discrete Wavelet Transform
QEWT	Quaternion Empirical Wavelet Transform
ART	Adaptive Resonance Theory
MAP	Mapping
MLP	Multi-Layer Perceptron
QSA	Quaternion Signal Analysis
V_h	Tangential mechanical vibration speed in the housing
V_a	Axial mechanical vibration speed on the driven side
V_s	Radial mechanical vibration speed on the non-driven side
V_d	Radial mechanical vibration speed on the driven side
$q(t)$	Quaternion signal in time domain
$q_d(t)$	Delayed quaternion in time domain
$q_r(t)$	Rotated quaternion in time domain
$\mathbf{w}[n]$	Windows vector
μ	Mean
RMSE	Root Mean Square Error

References

1. Aguayo-Tapia, S.; Avalos-Almazan, G.; Rangel-Magdaleno, J.d.J.; Ramirez-Cortes, M.J. Physical variable measurement techniques for fault detection in electric motors. *Energies* **2023**, *16*, 4780. [CrossRef]
2. Chen, J.; Wang, J.; Zhu, J.; Lee, T.H.; de Silva, C.W. Unsupervised Cross-Domain Fault Diagnosis Using Feature Representation Alignment Networks for Rotating Machinery. *IEEE ASME Trans. Mech.* **2021**, *26*, 2770–2781. [CrossRef]
3. Zheng, H.; Wang, R.; Yin, J.; Li, Y.; Lu, H.; Xu, M. A new intelligent fault identification method based on transfer locality preserving projection for actual diagnosis scenario of rotating machinery. *Mech. Syst. Signal Process.* **2020**, *135*, 106344. [CrossRef]
4. Altaf, S.; Ahmad, S.; Zaindin, M.; Huda, S.; Iqbal, S.; Soomro, M.W. Multiple industrial induction motors fault diagnosis model within powerline system based on wireless sensor network. *Sustainability* **2022**, *14*, 10079. [CrossRef]
5. Gu, B.G. Development of broken rotor bar fault diagnosis method with sum of weighted fourier series coefficients square. *Energies* **2022**, *15*, 8735. [CrossRef]
6. Gangsar, P.; Tiwari, R. Signal-based condition monitoring techniques for fault detection and diagnosis of induction motors: A state-of-the-art review. *Mech. Syst. Signal Process.* **2020**, *144*, 106908. [CrossRef]

7. Aguayo-Tapia, S.; Avalos-Almazan, G.; Rangel-Magdaleno, J.d.J.; Paternina, M.R.A. Broken bar fault detection using taylor-fourier filters and statistical analysis. *Entropy* **2023**, *25*, 44. [CrossRef] [PubMed]
8. Ibrahim, A.; Anayi, F.; Packianather, M.; Alomari, O.A. New hybrid invasive weed optimization and machine learning approach for fault detection. *Energies* **2022**, *15*, 1488. [CrossRef]
9. Yaman, O. An automated faults classification method based on binary pattern and neighborhood component analysis using induction motor. *Measurement* **2021**, *168*, 108323. [CrossRef]
10. Godoy, W.F.; da Silva, I.N.; Goedtel, A.; Palácios, R.H.C.; Lopes, T.D. Application of intelligent tools to detect and classify broken rotor bars in three-phase induction motors fed by an inverter. *IET Electr. Power Appl.* **2016**, *10*, 430–439. [CrossRef]
11. Nascimento, N.M.M.e.; Medeiros, C.M.S.; Filho, P.P.R. A comparison of machine learning methods to identify broken bar failures in induction motors using statistical moments. *Adv. Intell. Syst. Comput.* **2018**, *736*, 124–133. [CrossRef]
12. Martinez-Herrera, A.L.; Ferrucho-Alvarez, E.R.; Ledesma-Carrillo, L.M.; Mata-Chavez, R.I.; Lopez-Ramirez, M.; Cabal-Yepez, E. Multiple fault detection in induction motors through homogeneity and kurtosis computation. *Energies* **2022**, *15*, 1541. [CrossRef]
13. Singh, M.; Shaik, A.G. Entropy-based broken rotor-bar fault detection and estimation of its severity in a three-phase induction motor. In Proceedings of the 2020 IEEE International Conference on Power Electronics, Drives and Energy Systems, Jaipur, India, 16–19 December 2020; pp. 1–6. [CrossRef]
14. Bejaoui, I.; Bruneo, D.; Xibilia, M.G. Remaining useful life prediction of broken rotor bar based on data-driven and degradation model. *Appl. Sci.* **2021**, *11*, 7175. [CrossRef]
15. Kartiwa, A.; Supriatna, A.K.; Rusyaman, E.; Sulaiman, J. Review of quaternion differential equations: Historical development, applications, and future direction. *Axioms* **2023**, *12*, 483. [CrossRef]
16. Huang, C.; Li, J.; Gao, G. Review of quaternion-based color image processing methods. *Mathematics* **2023**, *11*, 2056. [CrossRef]
17. Abbassi, R.; Jerbi, H.; Kchaou, M.; Simos, T.E.; Mourtas, S.D.; Katsikis, V.N. Towards higher-order zeroing neural networks for calculating quaternion matrix inverse with application to robotic motion tracking. *Mathematics* **2023**, *11*, 2756. [CrossRef]
18. Li, J.; Chen, P.; Chang, Z.; Zhang, G.; Guo, L.; Zhao, C. Trajectory tracking control of quadrotor based on fractional-order s-plane model. *Machines* **2023**, *11*, 672. [CrossRef]
19. Rikam, L.E.; Bitjoka, L.; Nketsa, A. Quaternion Fourier transform spectral analysis of electrical currents for bearing faults detection and diagnosis. *Mech. Syst. Signal Process.* **2022**, *168*, 108656. [CrossRef]
20. Zhang, K.; Deng, Y.; Chen, P.; Ma, C.; Xu, Y. Quaternion empirical wavelet transform and its applications in rolling bearing fault diagnosis. *Measurement* **2022**, *195*, 111179. [CrossRef]
21. Contreras-Hernandez, J.L.; Almanza-Ojeda, D.L.; Ledesma-Orozco, S.; Garcia-Perez, A.; Romero-Troncoso, R.J.; Ibarra-Manzano, M.A. Quaternion Signal Analysis Algorithm for Induction Motor Fault Detection. *IEEE Trans. Ind. Electron.* **2019**, *66*, 8843–8850. [CrossRef]
22. Contreras-Hernandez, J.L.; Almanza-Ojeda, D.L.; Ledesma, S.; Garcia-Perez, A.; Castro-Sanchez, R.; Gomez-Martinez, M.A.; Ibarra-Manzano, M.A. Geometric analysis of signals for inference of multiple faults in induction motors. *Sensors* **2022**, *22*, 2622. [CrossRef] [PubMed]
23. Contreras-Hernandez, J.L.; Almanza-Ojeda, D.L.; Ibarra-Manzano, M.A.; Amezquita-Sanchez, J.P.; Valtierra-Rodriguez, M.; Camarena-Martinez, D. Short-Circuit Damage Diagnosis in Transformer Windings Using Quaternions: Severity Assessment through Current and Vibration Signals. *Appl. Sci.* **2023**, *13*, 12622. [CrossRef]
24. Cardenas-Cornejo, J.J.; Ibarra-Manzano, M.A.; González-Parada, A.; Castro-Sanchez, R.; Almanza-Ojeda, D.L. Classification of inter-turn short-circuit faults in induction motors based on quaternion analysis. *Measurement* **2023**, *222*, 113680. [CrossRef]
25. Sinha, A.K.; Das, S.; Chatterjee, T.K. Empirical relation for broken bar determination in scim. *COMPEL-Int. J. Comput. Math. Electr. Electron. Eng.* **2018**, *37*, 242–265. [CrossRef]
26. Talebi, S.P.; Werner, S.; Mandic, D.P. Quaternion-valued distributed filtering and control. *IEEE Trans. Autom. Control* **2020**, *65*, 4246–4257. [CrossRef]
27. Treml, A.E.; Flauzino, R.A.; Suetake, M.; Maciejewski, N.A.R. Experimental database for detecting and diagnosing rotor broken bar in a three-phase induction motor. *IEEE Dataport* **2020**. [CrossRef]
28. Ren, T.; Kang, X.; Sun, W.; Song, H. Study of Dynamometer Cards Identification Based on Root-Mean-Square Error Algorithm. *Int. J. Pattern Recognit. Artif. Intell.* **2018**, *32*, 1850004. [CrossRef]

Disclaimer/Publisher's Note: The statements, opinions and data contained in all publications are solely those of the individual author(s) and contributor(s) and not of MDPI and/or the editor(s). MDPI and/or the editor(s) disclaim responsibility for any injury to people or property resulting from any ideas, methods, instructions or products referred to in the content.